coatings

MDPI

Article

Boosting the Anti-Infection Ability of Titanium Implants by Coating Polydopamine–Curcumin

Manlong Chen [1], Wenyi Yu [1,2], Qi Shi [1,2], Han Wen [1], Guojing Li [1,2], Yunliang Wang [1,*], Tao Wang [1,2], Shibin Liu [1,2] and Tingting Yang [1,2,*]

[1] School of Pharmacy, Jiamusi University, Jiamusi 154007, China; cml15246475292@163.com (M.C.)
[2] Key Lab of Oral Biomedical Materials and Clinical Application of Heilongjiang Province, Jiamusi University, Jiamusi 154007, China
* Correspondence: jmswyl@126.com (Y.W.); yangtt@jmsu.edu.cn (T.Y.)

Abstract: To reduce the risk of infection, improving the anti-infection ability of Ti-based implantation has become a very meaningful task. In this work, by employing polydopamine (PDA) as a carrier and curcumin (CUR) as an anti-biotic/inflammatory, a series of Ti-PDA@CURx (x = 0.5, 1.0, 1.5, 2.0, 2.5) was successfully fabricated and characterized by scanning electron microscopy, Fourier transform infrared spectrometry, X-ray diffraction, X-ray photoelectron spectroscopy, and the water contact angle, where Ti plates were firmly coated by PDA@CUR. The test result of CUR content shows that the maximum loading of CUR in PDA can reach 0.6506%, where the CUR concentration is 1.5 mg/mL. The antibacterial test results demonstrate that Ti-PDA@CUR-x (x = 0.5, 1.0, 1.5, 2.0, 2.5) exhibit significant antibacterial activities against *Escherichia coli* and *S. aureu*, where Ti-PDA@CUR1.5 has the highest antibacterial rate of 62.7% against *Escherichia coli* and 52.6% against *S. aureus*. The cytotoxicity test shows that Ti-PDA, Ti-PDA@CUR-x (x = 0.5, 1.0, 1.5, 2.0, 2.5) has almost no toxicity.

Keywords: titanium; polydopamine; curcumin; antibacterial effect

Citation: Chen, M.; Yu, W.; Shi, Q.; Wen, H.; Li, G.; Wang, Y.; Wang, T.; Liu, S.; Yang, T. Boosting the Anti-Infection Ability of Titanium Implants by Coating Polydopamine–Curcumin. *Coatings* **2024**, *14*, 640. https://doi.org/10.3390/coatings14050640

Academic Editor: Ajay Vikram Singh

Received: 6 May 2024
Revised: 16 May 2024
Accepted: 16 May 2024
Published: 18 May 2024

1. Introduction

Because of their excellent mechanical properties, corrosion resistance, and biocompatibility, Ti-based implants have received increasing attention in dentistry, bone integration, and joint replacement surgery [1–4]. However, it was found that approximately 5% of patients receiving treatment were infected with bacteria after surgery because Ti-based implants do not have antibacterial properties [5–8]. To reduce the risk of implant infection, antibiotics are frequently introduced into Ti-based implantation [9], but just like the two sides of a coin, the overuse of antibiotics can result in the emergence of antibiotic-resistant bacteria in patients [10–13]. Once bacterial infection occurs, it can lead to implant failure, which requires surgical removal, resulting in surgical failure and economic losses [14]. Therefore, many antibacterial agents have been loaded on a Ti substrate to fabricate an antibacterial coating, and thereby, the antibacterial ability of Ti-based implants has been greatly improved, including metal [15,16] compounds/metal ions/nanoparticles [17] and antibiotics [18]. However, the use of metal layers as antibacterial agents may generate many side effects on the body's immunity and metabolism [19,20]. Therefore, developing a new coating for Ti-based implants with antibacterial properties and no cytotoxicity is very necessary.

Curcumin (CUR), a component abstracted from turmeric, possesses antibacterial [21,22], anti-inflammatory [23], and anti-tumor effects [24,25]. It is cost-effective, safe, and efficient, with minimal side effects, making it particularly well-suited for use in antibacterial applications [26]. However, curcumin is difficult to load tightly and heavily with Ti-based implants, as curcumin molecules contain multiple double bonds, as well as active groups such as phenolic hydroxyl and carbonyl groups, which can chemically bind with most compounds [27]. Its structure is shown in Figure 1 (right). It is well known that dopamine

can undergo oxidation and self-polymerization to create a polydopamine (PDA) coating that covers nearly every solid surface under alkaline conditions. In 2012, PDA was first discovered to be essential for the adhesion of sessile mussels [28] because catechol and primary amine, the functional groups of PDA, have better adhesion and antioxidant properties compared with others [29,30]. Its structure is shown in Figure 1 (left). Moreover, PDA is a commonly used drug carrier with good stability, hydrophilicity, and biocompatibility [31,32]. Considering the facts mentioned above, herein, by employing PDA as a carrier and CUR as an anti-biotic/inflammatory, a series of Ti-PDA@CUR was designed and fabricated, and the CUR loading contents (Ti-PDA@CUR-x (x = 0.5, 1.0, 1.5, 2.0, 2.5) were explored. More importantly, Ti-PDA@CURx exhibit excellent antibacterial activities against *Escherichia coli* and *S. aureu* and no toxicity. This work offers a promising research direction for the clinical application of antibacterial Ti-based implants.

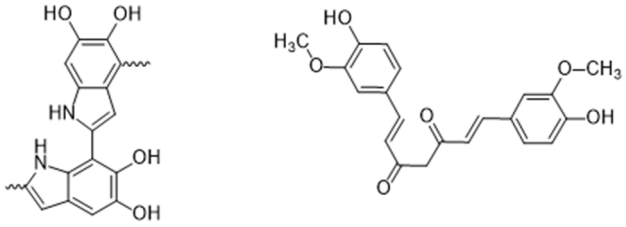

Figure 1. The open structures of polydopamine (**left**) and curcumin (**right**).

This study employs a simple and effective method for modifying CUR on the surface of titanium metal in order to explore the antibacterial effect of a CUR coating on *Escherichia coli* and *Staphylococcus aureus*, as well as the cytotoxic effect on osteoblast 3T3-E1.

2. Materials and Methods

2.1. Materials and Specimen Fabrication

Pure titanium plates for commercial use (Cp Ti; TA1, purity > 99.85%) measuring $10 \times 10 \times 1$ mm^3 were utilized. Each Ti plate was ultrasonically cleaned with a cleaning solution (V_{HF}:V_{HNO_3}:V_{H_2O} = 1:5:34). Initially, 1.21 g Tris (China Pharmaceutical Group, Shanghai, China) was weighed and placed in a 1 L beaker. Approximately 800 mL of deionized water was added to the beaker and stirred thoroughly to dissolve. The pH was adjusted to 8.5 using 1% hydrochloric acid, and the solution was brought to 1 L followed by the preparation of a 2 mg/mL dopamine solution by dissolving dopamine hydrochloride (McLean Reagent Co., Ltd., Shanghai, China) in a Tris–HCl buffer solution. Afterward, the titanium plate was immersed in a dopamine solution for 24 h. The soaking process was carried out on a constant temperature shaker at a constant speed, avoiding light vibrations. Next, the sample was rinsed with DI water to produce Ti-PDA after 24 h. Finally, Ti-PDA, as the substrate, was immersed in a CUR solution (0.5 mg/mL, 1.0 mg/mL, 1.5 mg/mL, 2.0 mg/mL and 2.5 mg/mL) for 24 h following the same preparation procedures and resulting in Ti-PDA@CUR0.5, Ti-PDA@CUR1.0, Ti-PDA@CUR1.5, Ti-PDA@CUR2.0, and Ti-PDA@CUR2.5.

2.2. Test of the CUR Content

The samples of Ti-PDA@CUR-x (x = 0.5, 1.0, 1.5, 2.0, 2.5) were sonicated in an ethanol solution to obtain five different concentrations of the CUR solution. The Ti sheets were placed in anhydrous ethanol to accelerate its release under ultrasound conditions. During this process, the solution was changed several times until it was released under ultrasound conditions, the Ti-PDA@CURx (x = 0.5, 1.0, 1.5, 2.0, 2.5) of the solution was clear and transparent, and there was no absorbance of the solution under a UV spectrophotometer. The absorbance was measured at 426 nm using a UV visible spectrophotometer (UV-5200 PC, Shanghai, China), and the CUR loading amount in the sample was determined by substituting the absorbance into the CUR standard curve. The calculation formula is as follows:

$$\text{CUR loading efficiency } (\%) = \frac{\text{Weight of the loaded CUR}}{\text{Weight of the initial sample}} \times 100\%$$

2.3. Surface Characterization

A scanning electron microscope (S4800HSD, Shimadzu Instrument Co., Ltd., Shimadzu, Japan) was used to examine the microstructure and morphology of Ti, Ti-PDA, and Ti-PDA@CUR1.5. Fourier transform infrared spectrometer was used to analyze Ti-PDA, CUR, and Ti-PDA@CUR1.5 between 500 and 4000 cm^{-1} (VERTEX70, Niton Spectrometer Company in the United States, Billerica, MA, USA) [33]. The diffraction patterns of Ti-PDA, CUR, and Ti-PDA@CUR1.5 were assessed using an X-ray diffractometer (Axios Petro, Panalytical, Co Kα, λ = 1.79021 (Worcestershire, UK)) in Cu-Kα, ranging from 5° to 50° (2θ). X-ray photoelectron spectroscopy (K-Alpha, Thermo Fisher Scientific, Waltham, MA, USA) was utilized to determine the elemental makeup of Ti-PDA, CUR, and Ti-PDA@CUR1.5 [34]. The hydrophilicity of the sample surfaces was measured by the water contact angle (SJ-210, Quantum Instrument Company, Suzhou, China).

2.4. In Vitro Antibacterial Tests

2.4.1. Bacterial Culture

Bacterial solutions of *E. coli* (ATCC 25922) and *S. aureus* (ATCC 25923) were streaked and inoculated on the surface of a nutrient agar plate with a 200 μL pipette tip, which was cultured in a bacterial culture incubator for 15 h. After passing to the third generation without impurities, they were used as experimental strains. The bacterial strains were removed and inoculated into nutrient an agar medium (TSB (McLean Biochemical Technology Co., Ltd., Shanghai, China) for Gram-positive bacteria and LB (McLean Biochemical Technology Co., Ltd., Shanghai, China) for Gram-negative bacteria) for cultivation for 5 h.

2.4.2. Preparation of Drug-Sensitive Tablets with Different Materials

Six groups of samples, including Ti-PDA, Ti-PDA@CUR0.5, Ti-PDA@CUR1.0, Ti-PDA@CUR1.5, Ti-PDA@CUR2.0, and Ti-PDA@CUR2.5, were immersed in a 0.9% saline solution and sonicated for drug release. Drug-sensitive paper (Shifeng Biotechnology Co., Ltd., Shanghai, China) pieces were added to the sample extraction solutions and immersed for 12 h for later use.

2.4.3. Bacteriostatic Rate Test

First, 60 μL of *E. coli* and *S. aureus* were inoculated at a concentration of 1×10^7 CFU/mL on the antimicrobial susceptibility tablets prepared as described above and grown in an incubator at 37 °C. After 24 h, the microbes present on the surface of the susceptibility tablets were rinsed with saline solution and then thinned to a concentration of 1×10^6 CFU/mL to create a bacterial suspension. Then, 100 μL of the diluted bacterial solution was inoculated on the agar plates, and the bacterial solution was spread evenly on the agar plates with the applicator. After incubation in a 37 °C incubator for 18 h, the agar plates with colonies were taken, and the number of colonies was measured using Image J 1.8.0 software.

$$\text{Bacteriost atic rate } (\%) = \frac{A - B}{A} \times 100\%$$

where A represents the number of colonies recovered from the Ti-PDA sample and B represents the number of colonies recovered from the test samples.

2.4.4. Zone of Inhibition

The resulting susceptibility tablets were pasted on the surface of *E. coli* and *S. aureus* agar plates. Plates with susceptibility tablets were incubated in a 37 °C incubator for 12 h to assess the antibacterial effectiveness of various samples against *E. coli* and *S. aureus*.

2.4.5. Bacterial Crystal Violet Staining

The antimicrobial properties of the susceptibility tablets were further assessed by bacterial biofilm crystal violet staining [35]. After preparing the groups of susceptibility tablets as described above, they were placed in 24-well plates. *E. coli* and *S. aureus* at a concentration of 1×10^6 CFU/mL were inoculated onto the tablet surfaces. The plates were incubated at 37 °C for 48 h before the bacteria were removed. Subsequently, the plates were washed thrice with PBS (McLean Reagent Co., Ltd., Shanghai, China, AR > 98%) to eliminate any inactive bacteria. Finally, 2.5% glutaraldehyde (McLean Reagent Co., Ltd., Shanghai, China) was added, and the samples were fixed at 4 °C for 4 h. After eliminating glutaraldehyde, 0.5% crystal violet dye was applied to every well plate for a duration of 2 h, and the residual dye solution was removed by washing the well plates three times with PBS. Pictures were taken to record the crystal violet staining in the different groups.

2.5. Cytotoxicity Test

DMEM medium (Bioengineering Co., Ltd., Shanghai, China) was set as a blank control group, and Ti-PDA, Ti-PDA@CUR0.5, Ti-PDA@CUR1, Ti-PDA@CUR1.5, Ti-PDA@CUR2, and Ti-PDA@CUR2.5 were set as the experimental groups. Each group of samples (three parallel samples per group) was placed on a super clean workbench, irradiated with ultraviolet light at a wavelength of 260 nm for 12 h, and then used later.

Experiments were performed on 3T3-E1 cells in the logarithmic growth phase, which were washed twice with PBS. First, 1 mL of trypsin cell digestion solution (0.25% trypsin) was added for 1 min, then 1 mL of DMEM medium was added to terminate digestion. The cell suspension was blown to form and centrifuged at 1000 rpm/min for 5 min. The supernatant was removed, and 1 mL of DMEM medium was added, blown to form cell suspension, and counted. The samples were placed in a 24-well plate in the order of grouping. The cells were inoculated into well plates at a density of 5×10^4 per well, and 500 μL cells per well were contained in DMEM complete culture medium after 48 h of cultivation in the incubator. The samples were removed and 20 μL of CCK-8 liquid and 180 μL of DMEM basic culture medium were added to each well, according to the instructions of the CCK-8 reagent kit, and gently shaken to make it uniform. Next, the cells were further grown in the incubator for 2 h. Subsequently, each group of solutions was moved to a 96-well plate, and the optical density (OD) of each sample in the wells was assessed using a microplate reader (BioTek-Infinire M200pro, Tecan, Männedorf, Switzerland) at a wavelength of 450 nm. The relative proliferation rate (RGR%) of 3T3-E1 cells was calculated. The calculation formula is as follows:

$$\mathrm{RGR\%} = \frac{\mathrm{ODe}}{\mathrm{ODc}} \times 100\%$$

where ODe represents the mean OD value of the experimental group, while ODc represents the mean OD value of the control group. According to the standards of the U.S. Pharmacopoeia, the cytotoxicity level (CTG) was evaluated, as shown in Table 1.

Table 1. Cytotoxicity rating table.

CTG	0	1	2	3	4
cytotoxicity	no	no	slight	medium	clear
RGR (%)	≥100	80~99	50~79	30~49	0~29

2.6. Statistical Analysis

The experimental data were analyzed statistically using SPSS (IBM SPSS Statistics 19) software, and the results were reported as the mean ± standard deviation.

3. Result and Discussion

3.1. Drug Loading Efficiency

Figures 2a and 2c, respectively, show the UV absorption spectra of CUR at 426 nm and the standard curves of CUR. In Figure 2b, as the concentration of CUR preparation solution increases, the loading of CUR in Ti-PDA significantly increases; when the CUR concentration is 1.5 mg/mL, the maximum loading of CUR in Ti-PDA reaches 0.6506%. When the CUR concentration exceeds 1.5 mg/mL, the loading of CUR in Ti-PDA shows a slow decreasing trend and finally tends to equilibrium at 2.5 mg/mL. Possible explanations are as follows: the catechol groups of CUR, and the primary amino groups of PDA can interact through hydrogen bonding [36], and the interaction force between CUR and PDA reaches the maximum or saturation when the CUR concentration is 1.5 mg/mL. As the concentration of CUR continues to increase, the repulsive force increases, hydrogen bonds weaken, and the loading decreases [37].

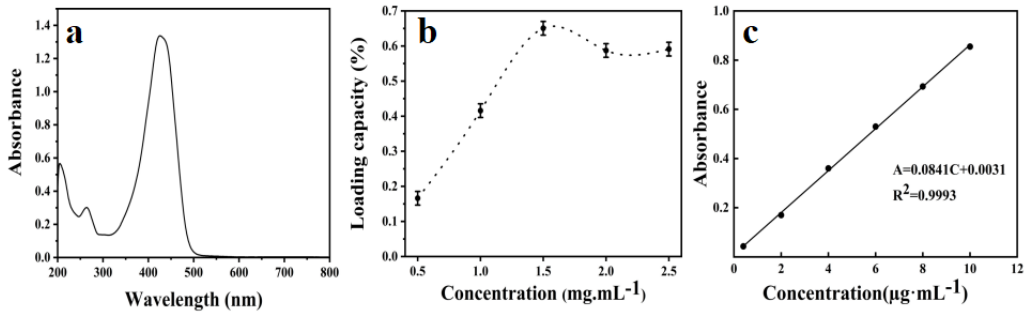

Figure 2. UV absorption spectrum of CUR (**a**), the loading amount of CUR on different Ti-PDA@CUR samples (**b**), and the CUR standard curve (**c**).

3.2. Characterization of Specimens

SEM images of Ti, Ti-PDA, and Ti-PDA@CUR1.5 are shown in Figure 3a–c. Compared with Ti, the surface of Ti-PDA is covered with a uniform layer of spherical nanoparticle coating. After loading CUR, block-shaped CUR can be clearly observed [38]. The FT-IR spectra of Ti-PDA, CUR, and Ti-PDA@CUR1.5 were also explored. As shown in Figure 3d, after CUR loading, new absorption peaks appear at 1607 cm^{-1} and 1508 cm^{-1} in Ti-PDA@CUR1.5, which are attributed to the vibrations of –C=O and –C=C in CUR. In addition, the peaks at 1000–1300 cm^{-1} can be assigned to the stretching vibrations of C–O–C in CUR [39]. Meanwhile, the peaks between 1000 and 1300 cm^{-1} may belong not only to C–O–C but also to C–O, C–C, and other functional groups. The peaks at about 900 and 650 cm^{-1} indicate interactions between Ti and oxygen (Ti-O) [40]. Furthermore, the peaks in the range of 3100–3500 cm^{-1} in Ti-PDA@CUR1.5 are more prominent than those of CUR, indicating the presence of strong bands related to the stretching vibration of –NH and –OH within PDA, unlike CUR [41]. As shown in Figure 3e, peaks at 18.98° and 27.81° are attributed to CUR and those at 12.13° originate from Ti-PDA [42], which can be observed in the XRD of Ti-PDA@CUR1.5, indicating crystalline CUR attached well to the Ti-PDA surface [43,44]. Based on the above experimental results, it is shown that the catechol group of CUR and the primary amino group of PDA successfully bind together under hydrogen bonding [36], proving that the Ti-PDA@CUR coating was successfully prepared.

Finally, the chemical composition of CUR, Ti-PDA, and Ti-PDA@CUR1.5 was investigated by XPS, and the survey spectra prove the coexistence of Ti, C, N, and O [34,41] (Figure 4a). The high-resolution spectra of C 1s could be fit with three peaks at ca. 284.8 eV and 286.1 eV, corresponding to C–C and C–O, respectively (Figure 4b). The deconvoluted peaks at ca. 400.0 eV, 401.6 eV, and 402.8 eV can be observed in the spectrum of N 1s (Figure 4c), which are attributed to –NH=, –NH–, and $–N^{+}H–$, respectively, where the –NH– bond serves as the connection between PDA and CUR [37]. Additionally, C=O and C–O bonds can be detected at 531.3 eV and 533.1 eV in the spectrum of O 1s (Figure 4d).

According to Yan's calculation method [33], compared with Ti-PDA, after coating CUR, the content of C–C bonds (59.4–28.1 eV) and C=O bonds (9.1–6.9 eV) decreased, and the content of –NH– bonds increased (31.8–67.2 eV) in Ti-PDA@CUR1.5, further indicating that the Ti-PDA@CUR composite was successful and there was a strong interaction force between them. Finally, the water contact angle of Ti-PDA and Ti-PDA@CUR1.5 was measured to test the hydrogen bond between the catechol group in CUR and PDA because the stronger the hydrophilicity, the stronger the hydrogen bond. The result shows that the order of the water contact angle is as follows: Ti (62.73°) > Ti-PDA (54.12°) > Ti-PDA@CUR1.5 (36.36°), which is consistent with the results presented above (Figure 4e–g).

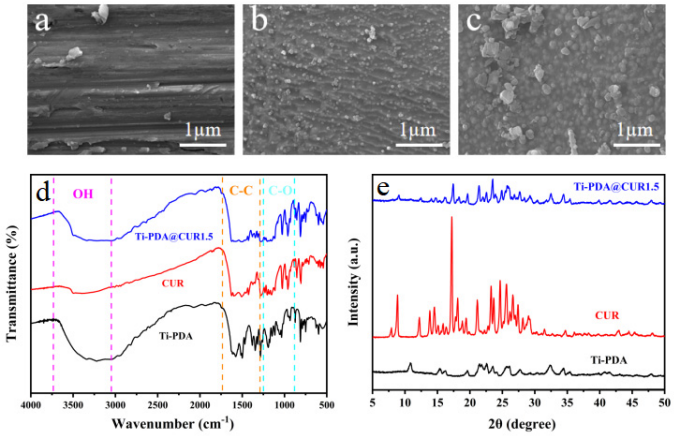

Figure 3. SEM images (**a**–**c**), FTIR spectra (**d**), and XRD (**e**) of Ti, Ti-PDA, CUR, and Ti-PDA@CUR1.5.

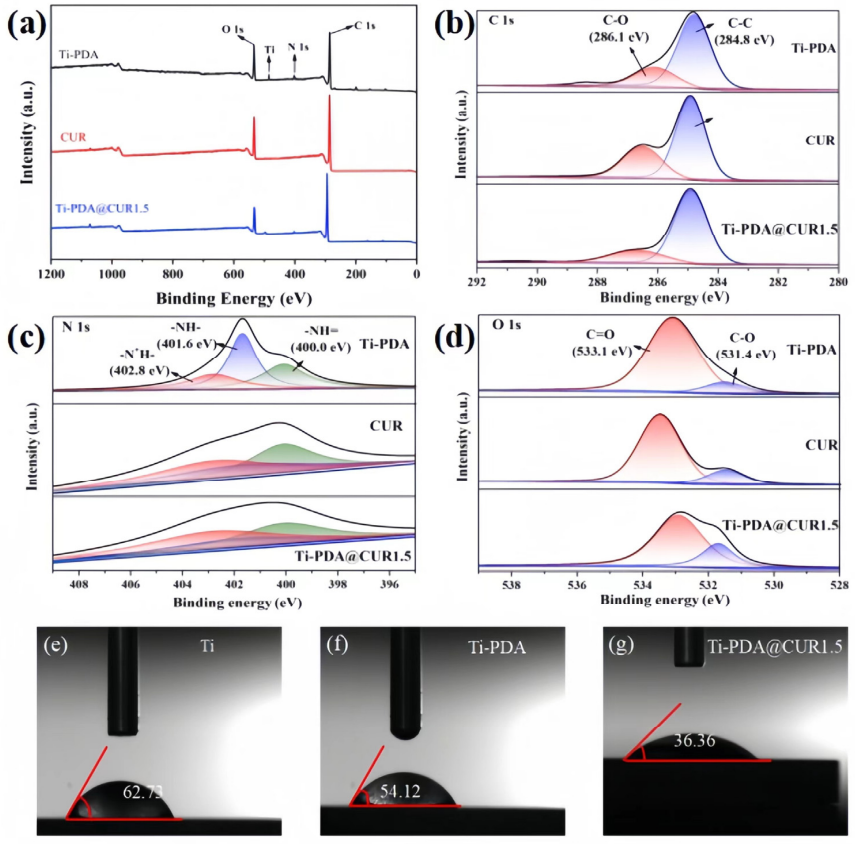

Figure 4. XPS full spectra of Ti-PDA, CUR, and Ti-PDA@CUR1.5 (**a**); C 1s (**b**), N 1s (**c**), and O 1s (**d**) high-resolution spectra of Ti-PDA@CUR1.5. The water contact angle of Ti (**e**), Ti-PDA (**f**), and Ti-PDA@CUR1.5 (**g**).

3.3. Antibacterial Activity

3.3.1. Bacterial Inhibition Rate

E. coli and *S. aureus* often cause infections with surgical implants [44]; therefore, the antibacterial properties of Ti-PDA@CURx (x = 0.5, 1.0, 1.5, 2.0, 2.5) were assessed by testing against Gram-negative *E. coli* and Gram-positive *S. aureus* using a standard spread plate technique on agar plates [45]. As shown in Figure 5a,b, the number of colonies in the Ti-PDA@CURx (x = 0.5, 1.0, 1.5, 2.0, 2.5) groups were significantly reduced compared with Ti-PDA. As the CUR content increases in Ti-PDA@CURx, there is a clear trend indicating that both the *E. coli* and *S. aureus* colonies decrease first and then increase. The bacteriostatic rates against *E. coli* and *S. aureus* in the experimental groups of Ti-PDA@CUR0.5, Ti-PDA@CUR1, Ti-PDA@CUR1.5, Ti-PDA@CUR2, and Ti-PDA@CUR2.5 are 11.4% and 9.3%, 34.7% and 26%, 62.7% and 52.6%, 59.3% and 44.0%, and 36.6% and 45.3%, respectively (Figure 5c,d). It is obvious that Ti-PDA@CURx (x = 0.5, 1.0, 1.5, 2.0, 2.5) possess broad-spectrum antibacterial ability. The optimal content of CUR is 1.5 mg/mL, and the antibacterial rates against *E. coli* and *S. aureus* can reach 62.7% and 52.6%, respectively.

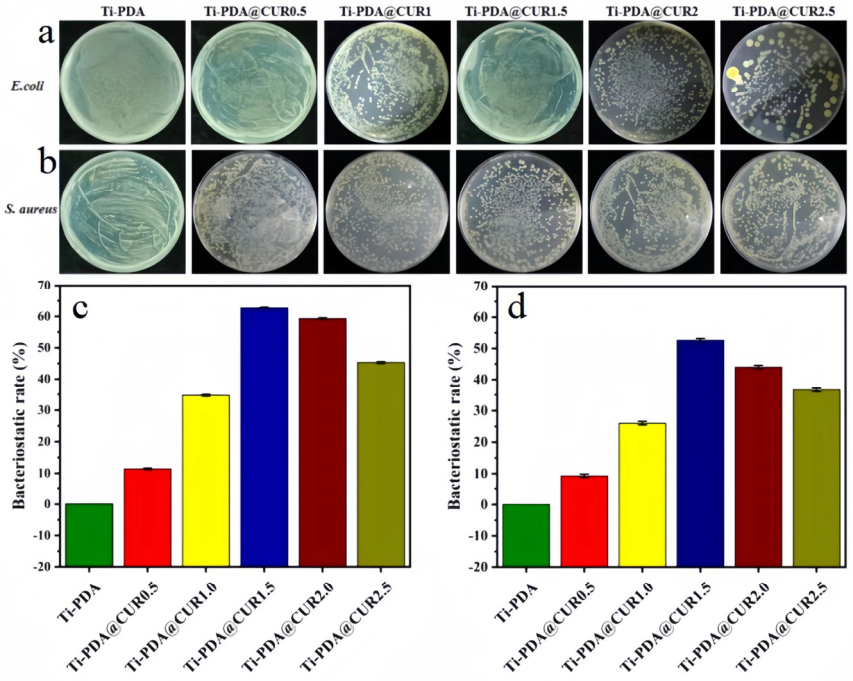

Figure 5. Optical images of agar plates showing the characteristic of the antibacterial activities (**a**,**b**) and the antibacterial rates (**c**,**d**) of Ti-PDA, Ti-PDA@CUR0.5, Ti-PDA@CUR1, Ti-PDA@CUR1.5, Ti-PDA@CUR2, and Ti-PDA@CUR2.5 against *E. coli* and *S. aureus*.

3.3.2. Zone of Inhibition Results

As shown in Figure 6a,b, compared with Ti-PDA, all Ti-PDA@CURx (x = 0.5, 1.0, 1.5, 2.0, 2.5) show a significant antibacterial circle. Consistent with the bacterial inhibition rate result, the diameter of the antibacterial ring shows an initial increase followed by a decrease with the increase in CUR content. More specifically, the diameter of the antibacterial circle against *E. coli* and *S. aureus* for Ti-PDA@CUR0.5, Ti-PDA@CUR1, Ti-PDA@CUR1.5, Ti-PDA@CUR2, and Ti-PDA@CUR2.5 is 9/9.3 mm, 12/10.3 mm, 17/17.5 mm, 16.3/15.3 mm, and 15/14.6 mm, respectively, where Ti-PDA@CUR1.5 exhibits the best antibacterial properties (Figure 6c,d). This may be because the phosphorylated groups with protonated amino groups in Ti-PDA@CUR interact electrostatically with phospholipid components of the cell membrane, potentially hindering bacteria from absorbing nutrients and multiplying [46].

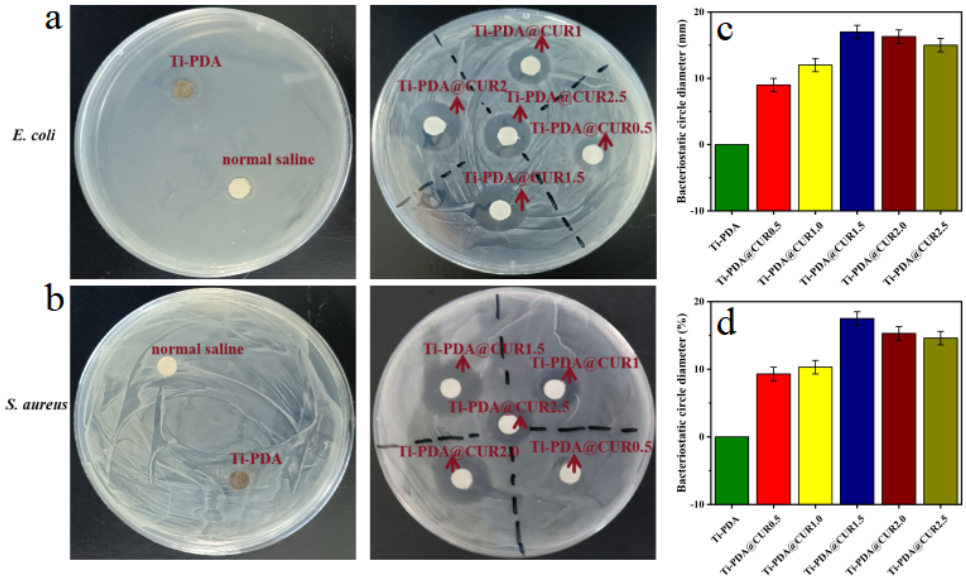

Figure 6. Antibacterial effect (**a**,**b**) and bacteriostatic circle diameter (**c**,**d**) of *E. coli* and *S. aureus* of the samples.

3.3.3. Bacterial Crystal Violet Staining Results

In clinical practice, *E. coli* and *S. aureus* are frequently encountered as pathogenic bacteria, and they tend to form bacterial biofilms at the site of infection [47]. In this experiment, the effects of antimicrobial susceptibility tablets on *E. coli* and *S. aureus* on bacterial biofilm formation were evaluated. As shown in Figure 7, the crystal violet color of the Ti-PDA@CUR sample became lighter compared with the Ti-PDA sample, and as the CUR content increased, it can be clearly seen that the crystal violet color of *E. coli* and *S. aureus* first lightened and then deepened. The color of *E. coli* in the Ti-PDA@CURx (x = 0.5, 1.0, 1.5, 2.0, 2.5) experimental groups first became lighter and then darkened. The color of *S. aureus* in the Ti-PDA@CURx (x = 0.5, 1.0, 1.5, 2.0, 2.5) experimental groups first became lighter and then darkened. At a loading drug concentration of 1.5 mg/mL, bacterial crystal violet was the lightest in color. This may be due to the saturation of hydrogen bond adsorption between 1.5 mg/mL CUR and Ti-PDA, which has the greatest electrostatic effect and prevents the reproduction of bacteria, so the antibacterial effect is the best.

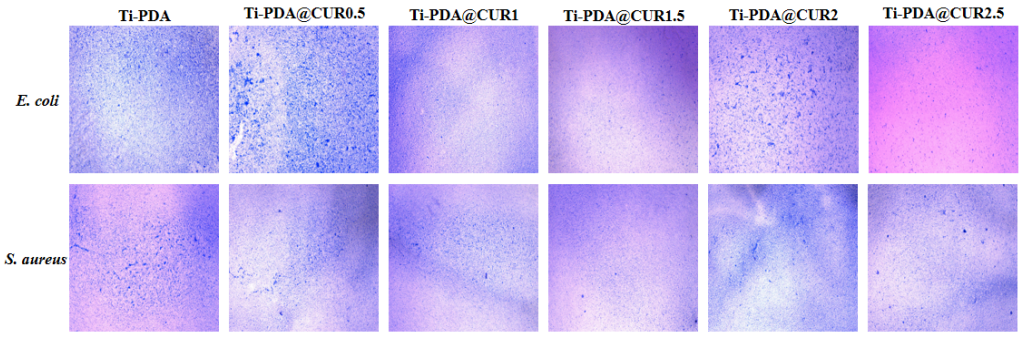

Figure 7. Effect of the samples on the preformed biofilm as assessed by crystal violet staining.

3.4. Cytotoxicity Test

Table 2 shows the corresponding cell proliferation rate (RGR%) and cytotoxicity level evaluations. The RGR% of Ti-PDA, Ti-PDA@CUR0.5, Ti-PDA@CUR1, Ti-PDA@CUR1.5, Ti-PDA@CUR2, and Ti-PDA@CUR2.5 are 80%–99%. The CTG levels are all at level 1. Thus, it can be determined that all the Ti-PDA@CUR samples are non-toxic.

Table 2. RGR% and cytotoxicity of 3T3-E1 cells after adding different samples.

Sample	RGR%	CTG	Cytotoxicity
Ti-PDA	90.0%	1	no
Ti-PDA@CUR0.5	89.7%	1	no
Ti-PDA@CUR1	93.2%	1	no
Ti-PDA@CUR1.5	94.7%	1	no
Ti-PDA@CUR2	88.7%	1	no
Ti-PDA@CUR2.5	89.2%	1	no

4. Conclusions

In short, new CUR coatings for Ti-based implants with antibacterial properties and no cytotoxicity, i.e., Ti-PDA@CURx (x = 0.5, 1.0, 1.5, 2.0, 2.5), were successfully fabricated. All results show that Ti-PDA@CURx (x = 0.5, 1.0, 1.5, 2.0, 2.5) are non-toxic and their antibacterial properties are superior to that of Ti-PDA. This may be because the phosphorylated groups with protonated amino groups in Ti-PDA@CUR interact electrostatically with the phospholipid components of the cell membrane, potentially hindering bacteria from absorbing nutrients and multiplying. Ti-PDA@CUR1.5 exhibits the best antibacterial effect on *E. coli* and *S. aureus*, with an inhibition rate of over 50%. This work illustrates that the CUR-loaded PDA coating possesses antibacterial effects and almost no toxicity, making it a potential option for orthopedic and dental implants.

Author Contributions: Formal analysis, T.Y., Y.W., Q.S. and M.C.; investigation, W.Y. and M.C.; writing—original draft preparation, M.C., G.L., H.W. and S.L.; review and editing, M.C., T.Y. and T.W. All authors have read and agreed to the published version of the manuscript.

Funding: This work was funded by the Talent Training Project of Reform and Development Funds of the Central Government Supporting Local Universities, grant number 2021zyzcdf-01, the Fundamental Research Business Expenses Fundamental Research Project of the Provincial Education Department Project of Heilongjiang Province of China, grant number 2021-KYYWF-0555, and the National Science Cultivation Foundation of Jiamusi University, grant number JMSUGPZR2022-019.

Institutional Review Board Statement: Not applicable.

Informed Consent Statement: Not applicable.

Data Availability Statement: The data are contained within this article.

Conflicts of Interest: All the authors declare no conflicts of interest.

References

1. Sarraf, M.; Rezvani Ghomi, E.; Alipour, S.; Ramakrishna, S.; Liana Sukiman, N. A state-of-the-art review of the fabrication and characteristics of titanium and its alloys for biomedical applications. *Bio-Des. Manuf.* **2022**, *5*, 371–395. [CrossRef]
2. Koizumi, H.; Takeuchi, Y.; Imai, H.; Kawai, T.; Yoneyama, T. Application of titanium and titanium alloys to fixed dental prostheses. *J. Prosthodont. Res.* **2019**, *63*, 266–270. [CrossRef]
3. Kanatsios, S.; Breik, O.; Dimitroulis, G. Biomet stock temporomandibular joint prosthesis: Long-term outcomes of the use of titanium condyles secured with four or five condylar fixation screws. *J. Craniomaxillofac. Surg.* **2018**, *46*, 1697–1702. [CrossRef]
4. Ding, Y.; Tao, B.; Ma, R.; Zhao, X.; Liu, P.; Cai, K. Surface modification of titanium implant for repairing/improving microenvironment of bone injury and promoting osseointegration. *J. Mater. Sci. Technol.* **2023**, *143*, 1–11. [CrossRef]
5. Ghimire, A.; Song, J. Anti-periprosthetic infection strategies: From implant surface topographical engineering to smart drug-releasing coatings. *ACS Appl. Mater. Interfaces* **2021**, *13*, 20921–20937. [CrossRef] [PubMed]
6. Zardi, E.M.; Franceschi, F. Prosthetic joint infection. A relevant public health issue. *J. Infect. Public Health* **2020**, *13*, 1888–1891. [CrossRef]
7. Schwarz, E.M.; McLaren, A.C.; Sculco, T.P.; Brause, B.; Bostrom, M.; Kates, S.L.; Parvizi, J.; Alt, V.; Arnold, W.V.; Carli, A.; et al. Adjuvant antibiotic-loaded bone cement: Concerns with current use and research to make it work. *J. Orthop. Res.* **2021**, *39*, 227–239. [CrossRef]
8. Stewart, P.S.; Bjarnsholt, T. Risk factors for chronic biofilm-related infection associated with implanted medical devices. *Clin. Microbiol. Infec.* **2020**, *26*, 1034–1038. [CrossRef]

9. Braem, A.; Kamarudin, N.H.N.; Bhaskar, N.; Hadzhieva, Z.; Mele, A.; Soulié, J.; Linklater, D.P.; Bonilla-Gameros, L.; Boccaccini, A.R.; Roy, I.; et al. Biomaterial strategies to combat implant infections: New perspectives to old challenges. *Int. Mater. Rev.* **2023**, *68*, 1011–1049. [CrossRef]
10. Darby, E.M.; Trampari, E.; Siasat, P.; Gaya, M.S.; Alav, I.; Webber, M.A.; Blair, J.M. Molecular mechanisms of antibiotic resistance revisited. *Nat. Rev. Microbiol.* **2023**, *21*, 280–295. [CrossRef]
11. Seemann, A.; Akbaba, S.; Buchholz, J.; Türkkan, S.; Tezcaner, A.; Woche, S.K.; Guggenberger, G.; Kirschning, A.; Dräger, G. RGD-modified titanium as an improved osteoinductive biomaterial for use in dental and orthopedic implants. *Bioconjugate Chem.* **2022**, *33*, 294–300. [CrossRef] [PubMed]
12. Su, K.; Tan, L.; Liu, X.; Cui, Z.; Zheng, Y.; Li, B.; Han, Y.; Li, Z.; Zhu, S.; Liang, Y.; et al. Rapid photo-sonotherapy for clinical treatment of bacterial infected bone implants by creating oxygen deficiency using sulfur doping. *ACS Nano* **2020**, *14*, 2077–2089. [CrossRef] [PubMed]
13. Abu Esba, L.C.; Al Mardawi, G.; AlJasser, M.I.; Aljohani, B.; Abu Alburak, A. Adverse drug reactions spontaneously reported at a tertiary care hospital and preventable measures implemented. *J. Clin. Pharm. Ther.* **2021**, *46*, 460–469. [CrossRef] [PubMed]
14. Zheng, T.X.; Li, W.; Gu, Y.Y.; Zhao, D.; Qi, M.C. Classification and research progress of implant surface antimicrobial techniques. *J. Dent. Sci.* **2022**, *17*, 1–7. [CrossRef] [PubMed]
15. Li, Q.; Yang, J.; Li, J.; Zhang, R.; Nakai, M.; Niinomi, M.; Nakano, T. Antibacterial Cu-doped calcium phosphate coating on pure titanium. *Mater. Trans.* **2021**, *62*, 1052–1055. [CrossRef]
16. Zhang, P.; Zhang, Z.; Li, W. Antibacterial TiO_2 coating incorporating silver nanoparticles by microarc oxidation and ion implantation. *J. Nanomater.* **2013**, *2013*, 2.
17. Luo, Q.; Cao, H.; Wang, L.; Ma, X.; Liu, X. ZnO@ZnS nanorod-array coated titanium: Good to fibroblasts but bad to bacteria. *J. Colloid Interface Sci.* **2020**, *579*, 50–60. [CrossRef]
18. Nie, B.E.; Long, T.; Ao, H.; Zhou, J.; Tang, T.; Yue, B. Covalent immobilization of enoxacin onto titanium implant surfaces for inhibiting multiple bacterial species infection and in vivo methicillin-resistant *Staphylococcus aureus* infection prophylaxis. Antimicrob. *Agents Chemother.* **2017**, *61*, 10–1128. [CrossRef]
19. Liu, J.; Zhao, H.; Wang, Y.; Shao, Y.; Zhang, L.; Xing, M. Impacts of simultaneous exposure to arsenic (III) and copper (II) on inflammatory response, immune homeostasis, and heat shock response in chicken thymus. *Int. Immunopharmacol.* **2018**, *64*, 60–68. [CrossRef]
20. Pohanka, M. Copper and copper nanoparticles toxicity and their impact on basic functions in the body. *Bratisl. Med. J.* **2019**, *120*, 397–409. [CrossRef]
21. Zheng, D.; Huang, C.; Huang, H.; Zhao, Y.; Khan, M.R.U.; Zhao, H.; Huang, L. Antibacterial mechanism of curcumin: A review. *Chem. Biodivers.* **2020**, *17*, e2000171. [CrossRef]
22. Dai, C.; Lin, J.; Li, H.; Shen, Z.; Wang, Y.; Velkov, T.; Shen, J. The natural product curcumin as an antibacterial agent: Current achievements and problems. *Antioxidants* **2022**, *11*, 459. [CrossRef] [PubMed]
23. Peng, Y.; Ao, M.; Dong, B.; Jiang, Y.; Yu, L.; Chen, Z.; Hu, C.; Xu, R. Anti-inflammatory effects of curcumin in the inflammatory diseases: Status, limitations and countermeasures. *Drug Des. Dev. Ther.* **2021**, *2021*, 4503–4525. [CrossRef] [PubMed]
24. Jahanbakhshi, F.; Maleki Dana, P.; Badehnoosh, B.; Yousefi, B.; Mansournia, M.A.; Jahanshahi, M.; Asemi, Z.; Halajzadeh, J. Curcumin anti-tumor effects on endometrial cancer with focus on its molecular targets. *Cancer Cell Int.* **2021**, *21*, 120. [CrossRef]
25. Ramezani, M.; Hatamipour, M.; Sahebkar, A. Promising anti-tumor properties of bisdemethoxycurcumin: A naturally occurring curcumin analogue. *J. Cell. Physiol.* **2018**, *233*, 880–887. [CrossRef] [PubMed]
26. Minhaco, V.M.T.R.; Huacho, P.M.M.; Imbriani, M.J.M.; Tonon, C.C.; Chorilli, M.; de Souza Rastelli, A.N.; Spolidorio, D.M.P. Improving antimicrobial activity against endodontic biofilm after exposure to blue light-activated novel curcumin nanoparticle. *Photodiagn. Photodyn. Ther.* **2023**, *42*, 103322. [CrossRef]
27. Lv, H.; Wang, Y.; Yang, X.; Ling, G.; Zhang, P. Application of curcumin nanoformulations in Alzheimer's disease: Prevention, diagnosis and treatment. *Nutr. Neurosci.* **2023**, *26*, 727–742. [CrossRef]
28. Gao, S.; Zhang, D.; Pedrero, M.; Guo, Z.; Pingarrón, J.M.; Campuzano, S.; Zou, X. Advances and opportunities of polydopamine coating in biosensing: Preparation, functionality, and applications. *Coord. Chem. Rev.* **2024**, *501*, 215564. [CrossRef]
29. Huang, S.; Liang, N.; Hu, Y.; Zhou, X.; Abidi, N. Polydopamine-assisted surface modification for bone biosubstitutes. *Biomed Res. Int.* **2016**, *2016*, 2389895. [CrossRef]
30. Liu, M.; Zeng, G.; Wang, K.; Wan, Q.; Tao, L.; Zhang, X.; Wei, Y. Recent developments in polydopamine: An emerging soft matter for surface modification and biomedical applications. *Nanoscale* **2016**, *8*, 16819–16840. [CrossRef]
31. Moraczewski, K.; Malinowski, R.; Laczny, D.; Macko, M. Surface modification of maize stem with polydopamine and tannic acid coatings. *Surf. Interfaces* **2021**, *26*, 101319. [CrossRef]
32. Jabbar, A.; Rehman, K.; Jabri, T.; Kanwal, T.; Perveen, S.; Rashid, M.A.; Kazi, M.; Ahmad Khan, S.; Saifullah, S.; Shah, M.R. Improving curcumin bactericidal potential against multi-drug resistant bacteria via its loading in polydopamine coated zinc-based metal-organic frameworks. *Drug Deliv. Transl.* **2023**, *30*, 2159587. [CrossRef]
33. Yan, H.; Li, P.; Jiang, X.; Wang, X.; Hu, Y.; Zhang, Y.; Su, R.; Su, W. Preparation of graphene oxide/polydopamine-curcumin composite nanomaterials and its antibacterial effect against *Staphylococcus aureus* induced by white light. *Biomater. Adv.* **2022**, *139*, 213040. [CrossRef]

34. Barak, T.; Sharon, E.; Steinberg, D.; Feldman, M.; Sionov, R.V.; Shalish, M. Anti-bacterial effect of cannabidiol against the cariogenic *Streptococcus mutans* bacterium: An In Vitro Study. *Int. J. Mol. Sci.* **2022**, *23*, 15878. [CrossRef]
35. Zeng, Y.; Luo, Y.; Wang, L.; Zhang, K.; Peng, J.; Fan, G. Therapeutic effect of curcumin on metabolic diseases: Evidence from clinical studies. *Int. J. Mol. Sci.* **2023**, *24*, 3323. [CrossRef]
36. Pan, H.; Shen, X.; Tao, W.; Chen, S.; Ye, X. Fabrication of polydopamine-based curcumin nanoparticles for chemical stability and pH-responsive delivery. *J. Agric. Food Chem.* **2020**, *68*, 2795–2802. [CrossRef]
37. Wang, H.; Zheng, C.; Tian, F.; Xiao, Z.; Sun, Z.; Lu, L.; Dai, W.; Zhang, Q.; Mei, X. Improving the dissolution rate and bioavailability of curcumin via co-crystallization. *Pharmaceuticals* **2024**, *17*, 489. [CrossRef]
38. Chen, D.; Yu, C.; Ying, Y.; Luo, Y.; Ren, L.; Zhu, C.; Yang, K.; Wu, B.; Liu, Q. Study of the osteoimmunomodulatory properties of curcumin-modified copper-bearing titanium. *Molecules* **2022**, *27*, 3205. [CrossRef]
39. Ghobadi, N.; Asoodeh, A. Co-administration of curcumin with other phytochemicals improves anticancer activity by regulating multiple molecular targets. *Phytother. Res* **2023**, *37*, 1688–1702. [CrossRef]
40. Baig, M.T.; Kayan, A. Eco-friendly novel adsorbents composed of hybrid compounds for efficient adsorption of methylene blue and Congo red dyes: Kinetic and thermodynamic studies. *Sep. Sci. Technol.* **2023**, *58*, 862–883. [CrossRef]
41. Maruthapandi, M.; Saravanan, A.; Das, P.; Natan, M.; Jacobi, G.; Banin, E.; Luong, J.H.T.; Gedanken, A. Antimicrobial activities of Zn-doped CuO microparticles decorated on polydopamine against sensitive and antibiotic-resistant bacteria. *ACS Appl. Polym. Mater.* **2020**, *2*, 5878–5888. [CrossRef]
42. Bai, Z.; Hu, K.; Shou, Z.; Yu, J.; Meng, H.; Zhou, H.; Chen, L.; Yu, T.; Lu, R.; Li, N.; et al. Layer-by-layer assembly of procyanidin and collagen promotes mesenchymal stem cell proliferation and osteogenic differentiation in vitro and in vivo. *Regen. Biomater.* **2023**, *10*, rbac107. [CrossRef] [PubMed]
43. Shahriari, M.; Kesharwani, P.; Johnston, T.P.; Sahebkar, A. Anticancer potential of curcumin-cyclodextrin complexes and their pharmacokinetic properties. *Int. J. Pharm.* **2023**, *631*, 122474. [CrossRef] [PubMed]
44. Liu, F.; Cheng, X.; Xiao, L.; Wang, Q.; Yan, K.; Su, Z.; Wang, L.; Ma, C.; Wang, Y. Inside-outside Ag nanoparticles-loaded polylactic acid electrospun fiber for long-term antibacterial and bone regeneration. *Int. J. Biol. Macromol.* **2021**, *167*, 1338–1348. [CrossRef] [PubMed]
45. Li, D.; Li, J.; Wang, S.; Wang, Q.; Teng, W. Dually crosslinked copper-poly (tannic acid) nanoparticles with microenvironment-responsiveness for infected wound treatment. *Adv. Healthc.* **2023**, *12*, 2203063. [CrossRef] [PubMed]
46. Manna, S.; Seth, A.; Gupta, P.; Nandi, G.; Dutta, R.; Jana, S.; Jana, S. Chitosan derivatives as carriers for drug delivery and biomedical applications. *ACS Biomater. Sci.* **2023**, *9*, 2181–2202. [CrossRef]
47. Hyderi, Z.; Nagarajan, H.; Priya, S.J.; Jeyakanthan, J.; Veera Ravi, A. Exploring the antimicrobial potential of 4, 5, 7-trihydroxyflavanone (THF) against vancomycin-resistant *Enterococcus gallinarum* infections: In vitro and in silico investigations. *J. Biomol. Struct. Dyn.* **2023**, *12*, 1–15. [CrossRef]